Opto-Electronic Science

ISSN 2097-0382 CN 51-1800/O4

Ultrafast dynamics of femtosecond laser-induced high spatial frequency periodic structures on silicon surfaces

Ruozhong Han, Yuchan Zhang, Qilin Jiang, Long Chen, Kaiqiang Cao, Shian Zhang, Donghai Feng, Zhenrong Sun and Tianqing Jia

Citation: Han RZ, Zhang YC, Jiang QL, et al. Ultrafast dynamics of femtosecond laser-induced high spatial frequency periodic structures on silicon surfaces. *Opto-Electron Sci* **3**, 230013 (2024).

https://doi.org/10.29026/oes.2024.230013

Received: 1 June 2023; Accepted: 3 November 2023; Published online: 4 February 2024

Related articles

Femtosecond laser-induced periodic structures: mechanisms, techniques, and applications

Yuchan Zhang, Qilin Jiang, Mingquan Long, Ruozhong Han, Kaiqiang Cao, Shian Zhang, Donghai Feng, Tianqing Jia, Zhenrong Sun, Jianrong Qiu, Hongxing Xu

Opto-Electronic Science 2022 **1**, 220005 doi: 10.29026/oes.2022.220005

Periodic transparent nanowires in ITO film fabricated via femtosecond laser direct writing

Qilin Jiang, Long Chen, Jukun Liu, Yuchan Zhang, Shian Zhang, Donghai Feng, Tianqing Jia, Peng Zhou, Qian Wang, Zhenrong Sun, Hongxing Xu

Opto-Electronic Science 2023 **2**, 220002 doi: 10.29026/oes.2023.220002

Three-dimensional isotropic microfabrication in glass using spatiotemporal focusing of high-repetition-rate femtosecond laser pulses

Yuanxin Tan, Haotian Lv, Jian Xu, Aodong Zhang, Yunpeng Song, Jianping Yu, Wei Chen, Yuexin Wan, Zhaoxiang Liu, Zhaohui Liu, Jia Qi, Yangjian Cai, Ya Cheng

Opto-Electronic Advances 2023 **6**, 230066 doi: 10.29026/oea.2023.230066

Microsphere femtosecond laser sub-50 nm structuring in far field via non-linear absorption

Zhenyuan Lin, Kuan Liu, Tun Cao, Minghui Hong

Opto-Electronic Advances 2023 **6**, 230029 doi: 10.29026/oea.2023.230029

More related article in Opto-Electronic Journals Group website

OES Opto-Electronic Science

http://www.oejournal.org/oes

OE_Journal

Website

Opto-Electronic Science

Article

March 2024, Vol. 3, No. 3

DOI: 10.29026/oes.2024.230013

Ultrafast dynamics of femtosecond laser-induced high spatial frequency periodic structures on silicon surfaces

Ruozhong Han[1], Yuchan Zhang[1], Qilin Jiang[1], Long Chen[2], Kaiqiang Cao[3], Shian Zhang[1], Donghai Feng[1], Zhenrong Sun[1] and Tianqing Jia[1,2,4]*

Femtosecond laser-induced periodic surface structures (LIPSS) have been extensively studied over the past few decades. In particular, the period and groove width of high-spatial-frequency LIPSS (HSFL) is much smaller than the diffraction limit, making it a useful method for efficient nanomanufacturing. However, compared with the low-spatial-frequency LIPSS (LSFL), the structure size of the HSFL is smaller, and it is more easily submerged. Therefore, the formation mechanism of HSFL is complex and has always been a research hotspot in this field. In this study, regular LSFL with a period of 760 nm was fabricated in advance on a silicon surface with two-beam interference using an 800 nm, 50 fs femtosecond laser. The ultrafast dynamics of HSFL formation on the silicon surface of prefabricated LSFL under single femtosecond laser pulse irradiation were observed and analyzed for the first time using collinear pump-probe imaging method. In general, the evolution of the surface structure undergoes five sequential stages: the LSFL begins to split, becomes uniform HSFL, degenerates into an irregular LSFL, undergoes secondary splitting into a weakly uniform HSFL, and evolves into an irregular LSFL or is submerged. The results indicate that the local enhancement of the submerged nanocavity, or the nanoplasma, in the prefabricated LSFL ridge led to the splitting of the LSFL, and the thermodynamic effect drove the homogenization of the splitting LSFL, which evolved into HSFL.

Keywords: laser-induced periodic surface structures (LIPSS); local field enhancement; collinear pump-probe imaging; silicon; high spatial frequency periodic structures

Han RZ, Zhang YC, Jiang QL et al. Ultrafast dynamics of femtosecond laser-induced high spatial frequency periodic structures on silicon surfaces. *Opto-Electron Sci* **3**, 230013 (2024).

Introduction

Over the past few decades, femtosecond lasers have been increasingly used in micro or nano processing because of their low thermal effects, high processing accuracy, and applicability to various materials[1,2]. An interesting phenomenon is the laser-induced periodic surface structure (LIPSS). By changing the laser fluence and cumulative pulse number, femtosecond lasers induce LIPSS with varying properties such as periods, depths, and regularity on various materials such as metals, semiconductors, and transparent dielectrics[3–7]. These periodic nanostructures

[1]State Key Laboratory of Precision Spectroscopy, School of Physics and Electronic Science, East China Normal University, Shanghai 200241, China; [2]Institute of Laser Manufacturing, Henan Academy of Sciences, Zhengzhou 450046, China; [3]Institute of Physics, Chinese Acadamy of Sciences, Beijing 100190, China; [4]Collaborative Innovation Center of Extreme Optics, Shanxi University, Taiyuan 030006, China.
*Correspondence: TQ Jia, E-mail: tqjia@phy.ecnu.edu.cn; h185723538@163.com
Received: 1 June 2023; Accepted: 3 November 2023; Published online: 4 February 2024

Open Access This article is licensed under a Creative Commons Attribution 4.0 International License.
To view a copy of this license, visit http://creativecommons.org/licenses/by/4.0/.

© The Author(s) 2024. Published by Institute of Optics and Electronics, Chinese Academy of Sciences.

have significant applications in surface structural color, information storage, enhanced emission and absorption, anisotropic conductivity, and the regulation of hydrophobic and hydrophilic characteristics[8–16].

Laser-induced periodic surface structure can be categorized into low spatial frequency LIPSS (LSFL, $\Lambda>\lambda/2$) and high spatial frequency LIPSS (HSFL, $\Lambda<\lambda/2$), where Λ and λ are the LIPSS period and laser wavelength, respectively[17,18]. Numerous experimental and theoretical studies have been conducted to understand the formation mechanism of LIPSS. The results indicated that the LSFL originates from surface plasmon polaritons (SPPs) excited by the incident laser or the interference modulation of scattered light and incident light, both of which lead to a periodic distribution of laser energy in space[19–21]. This can cause periodic absorption and ablation of the surface material, thereby forming periodic nanostructures.

However, compared to the LSFL, the structure size of the HSFL is smaller, its morphology is more irregular. After solidification, due to the hydrodynamic effects of the molten layer, transient HSFL was more likely to be submerged, similar to the cases occurred in LSFL on the gold surface[22,23]. Therefore, the formation mechanism of the HSFL is complex and has been a crucial subject in the last few decades. The following models have been proposed to explain the formation mechanism of the HSFL.

A thin plasma layer is excited on a surface irradiated with a femtosecond laser[24]. The thin-film model suggests that the HSFL originated from the SPP on the lower surface of the plasma layer or from the coupled waves of the upper and lower SPP of the thin plasma layer[25–28]. A thin, highly nonequilibrium layer of molten liquid is formed on the surface of the material excited using a femtosecond laser. The self-organization model proposes that fluid dynamics instability[29–31], coherent cavitation of the melt[32,33], or stress relaxation via diffusing defects[34] in the liquid layer result in the formation of the HSFL. The local enhancement model encompasses the asymmetric field enhancement of nano plasma[35], the local field enhancement of ripple ridges[36], or the localized field enhancement caused by surface roughness[37–39]. Huang et. al. demonstrated that in ultrafast laser ablation of ZnO, Si, and GaAs, the plasmonic effects play an important role in the phenomenon of laser-induced grating splitting towards the nanoscale, which provides a straightforward way for the formation of HSFL structures[40,41]. The high-harmonic model suggests that high harmonic generation is responsible for the HSFL formation[5,42]. Surface scattered second harmonic generation was observed in the regime of HSFL formation on ZnO crystal[42]. This model explained well the spatial periods, the orientation, and different angular dependence of HSFL structures.

Several studies show that the formation of LIPSS depends not only on the distribution of the laser field but also on the ablation process and the thermal and fluid dynamics of materials[43–45]. All these factors have a significant impact on the LIPSS morphology, which is significantly different from its initial electromagnetic origin[46]. SEM, TEM, and AFM are widely used to study the HSFL after solidification, but these methods cannot observe the transient nanostructures during the formation of LIPSS[47]. K. Cheng observed the ultrafast dynamics on gold film surfaces using a collinear pump-probe imaging system and discovered a clear and regular transient LSFL induced by a single femtosecond pulse[23]. These transient LSFLs were ultimately submerged during the solidification process because of the strong thermal effect.

The HSFL period was shorter and more sensitive to thermodynamic effects during laser ablation. The mechanism of HSFL formation remains unclear and is a challenging topic. Therefore, developing high-spatial-resolution ultrafast imaging methods is meaningful as well as necessary to study the dynamics of HSFL formation.

Typically, HSFL is formed after irradiation with multiple femtosecond laser pulses[48]. However, the ablated debris and remelted materials deposited on the surface significantly disturbed the distribution of the subsequent laser field through the scattering light field or excitation of the SPP. Moreover, the thermal accumulation and hydrodynamic effects of multi-pulse laser ablation are complex, creating additional challenges in understanding the formation mechanism of the HSFL.

In this study, we prepared a regular and uniform LSFL with a period of 760 nm on a silicon surface using a two-beam interference method using a femtosecond laser with a central wavelength of 800 nm and a pulse width of 50 fs. The ultrafast dynamics of HSFL formation on the silicon surface of prefabricated LSFL under single femtosecond laser pulse irradiation were observed and analyzed for the first time using collinear pump-probe imaging method. In general, under laser irradiation with different fluences, the evolution of the surface structure occurs in five sequential stages: LSFL begins to split, becomes a uniform HSFL, degenerates into an irregular LSFL, undergoes secondary splitting into a

weakly uniform HSFL, and evolves into an irregular LSFL or is submerged. The results indicate that the local enhancement of the submerged nanocavity, or the nanoplasma, in the prefabricated LSFL ridge led to the splitting of the LSFL, and the thermodynamic effect drove the homogenization of the splitting LSFL, which evolved into HSFL.

Experiment

Sample

The sample used in this study was a commercial undoped silicon wafer (100) (China MTI Corporation) with a diameter of 100 mm and a thickness of 0.5 mm. The surface was optically polished to a roughness of less than 1 nm. After laser irradiation, the sample is immersed in deionized water and cleaned with an ultrasonic cleaner for 15 minutes to remove dust and nanoparticle deposited on the surface.

Prefabricated LSFL on the surface of silicon

The laser system was a commercial Ti:Sapphire regenerative amplifier (Legend Elite, Coherent), which generated laser pulses at 800 nm, 50 fs, and 3.5 mJ at a repetition rate of 1000 Hz. A dual-beam interference system is established by focusing the two laser beams with two vertically positioned cylindrical lenses, resulting in a focal spot with a width of 50 μm and a length of 7.0 mm. The angle between the two laser beams is adjusted to 63.4°, which makes the interference period $\Lambda = \lambda/(2\sin(\theta/2)) = 761$ nm, approximately equal and parallel to the period of surface plasmon polaritons (SPP) and leads to coherent resonant enhancement of the SPP. This method is beneficial for the growth of ideal LSFL patterns, reducing the irregularity caused by disturbances from previous pulse ablations and thus quickly forming regular and uniform LSFL patterns[49].

Confocal optical microscopy (COM) (ZEISS Smartproof 5 Widefield Confocal Microscope) was used to measure surface morphology. Figure 1 shows a COM image of the LSFL prefabricated on a silicon surface by direct writing with dual-beam interference, where a single-beam laser with a fluence of 0.13 J/cm^2 and a scanning speed of 2 mm/s. The average cumulative number of laser pulses is 25 for the preparation of LSFL. The LSFL was regular and uniform, with a period of 760 nm and a depth of 14 nm.

Collinear pump-probe imaging system

The ultrafast dynamics of the formation process of HSFL on silicon induced by a femtosecond laser were studied using a collinear pump-probe imaging technique, as shown in Fig. 2[50]. A single pulse acting on the sample was selected using an electric shutter, and the energy was adjusted using a continuous attenuator composed of a half-wave plate and a polarized beam splitter. The laser was split into two beams by using a 50% beam splitter. One was used as the pump beam, which passed through a delay line, and was focused on the sample surface using a 100× objective lens to induce the formation of HSFL. The other beam was used as the probe beam, and was focused onto a water cell via a convex lens to generate white light. The light was then collimated by another convex lens, and the spectrum was cut down from the original range of 450–950 nm to 450–570 nm using a 550 nm low-pass filter, as shown in Fig. 2(b). The probe and pump beams were collinear using a beam combiner, passed through a concave lens, and illuminated the sample through a 100× objective lens (*NA*=0.9). Another 550 nm low-pass filter was placed in front of the CCD to block the 800 nm laser reflected from the sample surface.

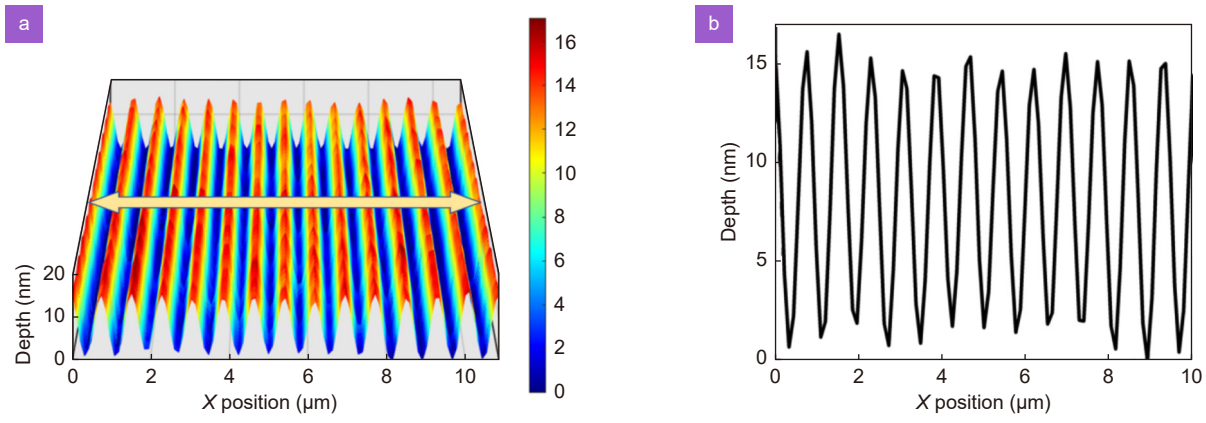

Fig. 1 | (**a**) Confocal optical microscopy image of LSFL prefabricated on silicon surface, and (**b**) cross-sectional profile of LSFL.

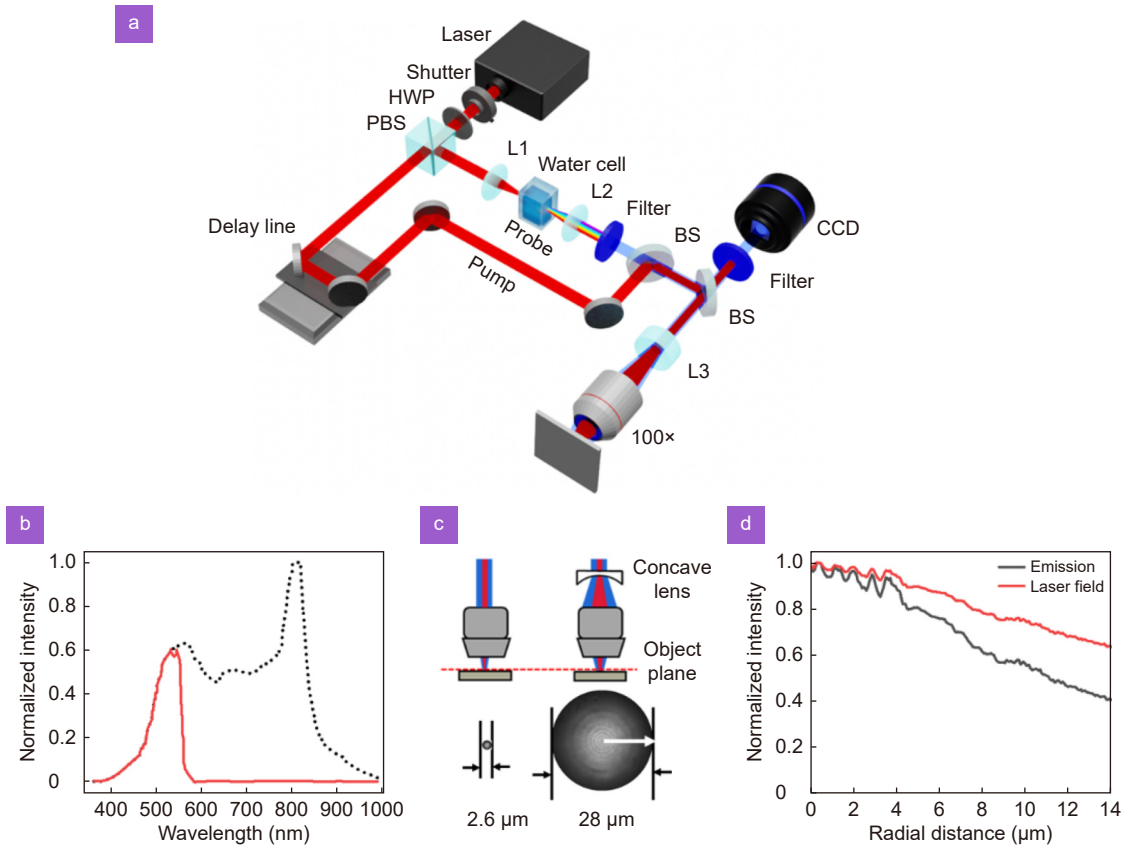

Fig. 2 | (**a**) Experiment setup of the collinear pump-probe imaging system; HWP is half wave plate, PBS is polarized beam splitter, and BS is beam splitter. (**b**) Spectra of the white-light pulse with (red solid curve) and without (black dotted curve) the short-wave-pass filter. (**c**) Laser spot area on the object plane with and without the concave lens. (**d**) The profile of the normalized intensity of blue light emission and laser field intensity along the arrow in (c).

The sample was placed on the object plane of the objective to achieve a clear image. However, under a 100× objective, the focal and object planes are very close; therefore, the ablation spot during laser irradiation is very small, with a diameter of only 2.6 μm, which is not sufficiently large to induce enough periodic ripples. The focus spot was enlarged to 28 μm in diameter by placing a concave lens with $f = -120$ mm in front of the objective. Meanwhile, the concave lens will cause the pump laser to diverge. When passing through a 100× objective lens, small aperture diffraction occurs due to the presence of the incident pupil, resulting in the diffraction rings (Fig. 2(c)).

The intensity distribution of laser field at the object plane is measured by a CCD camera via the emission light from a CdS crystal. The laser field intensity should be the square root of the blue light intensity, as blue light emission is a two-photon absorption process of 800 nm light. Fig. 2(c) and 2(d) show that there are several diffraction rings in the inner region for radius $r < 6$ μm, where the laser field intensity fluctuates significantly. However, in the outer region for radius 6 μm $< r <$ 14 μm, the laser intensity gradually decreases to 0.63. The laser intensity changes smoothly without significant fluctuations.

The spectral parameters of white light determine the temporal and spatial resolutions of an experimental setup. In this experiment, the spectral range of white light was 450–570 nm, corresponding to a spatial resolution of 250–317 nm. The pulse width of the white light illuminated on the sample surface was estimated to be 0.6 ps[51]. Owing to the limitations of spatial resolution, this study mainly reports the ultrafast dynamics of HSFL with periods larger than 300 nm.

Silicon with a prefabricated LSFL was placed on an $x/y/z$ translation stage to perform an ultrafast imaging experiment on the laser induced HSFL. After each laser exposure, the sample was transferred to a fresh area for other experiments.

Results and discussion

In this section, we investigate the ultrafast imaging and

dynamic process of HSFL formation on a silicon surface with a prefabricated LSFL induced by a single femtosecond laser pulse.

Solidified surface structures after irradiated by a single femtosecond laser pulse with different fluence

Figure 3 shows optical microscopic images of typical surface structures on silicon with a prefabricated LSFL before and after single-laser pulse irradiation. When the laser fluence is within the range of 0.48–0.88 J/cm^2, the initially prepared LSFL on the silicon surface exhibits significant bending and fracture, whereas the overall structure remains as the LSFL pattern. The width of LSFL ripple after solidification is measured with SEM image. When the laser fluence is 0.48 J/cm^2, it increases from 550 nm to 619 nm due to the local enhancement of the laser field at the center of the LSFL ridge[40,52]. It then decreases to 368 nm for the strong ablation when the laser fluence increases to 0.88 J/cm^2. When the laser fluence is greater than 0.88 J/cm^2, severe ablation and melting occur, and the LSFL patterns are submerged. The experimental results showed that after surface solidification, no obvious regular HSFL patterns were observed after single-pulse laser irradiation, regardless of the laser fluence. These results are consistent with those of several studies stating that the HSFL pattern is mainly induced by the accumulation of multiple pulses with low fluence.

Ultrafast dynamics of the formation of HSFL irradiated by a single pulse with a fluence of 0.82 J/cm^2

Generally, the formation of HSFL on a solidified surface is observed by scanning electron microscopy or atomic force microscope[53,54]. These methods are effective in detecting the periodicity, morphology, and composition of the retained HSFL; however, they cannot observe the transient process of HSFL formation. Many studies have reported that HSFL can be formed under low-fluence and multi-pulse laser irradiation but cannot be induced by a few high-fluence pulses, which makes it more complex and difficult to explain the formation of HSFL[55,56]. Moreover, although no preserved HSFL was observed after high-fluence laser irradiation, this did not mean that a transient HSFL never formed. In this study, we investigated the formation of SFL on the silicon surface of a prefabricated LSFL under single femtosecond laser pulse irradiation using collinear pump-probe imaging.

Figure 4 shows the transient images of the silicon surface with the prefabricated LSFL after single-pulse irradiation at different delay times. The laser fluence was 0.82 J/cm^2, which is significantly higher than the ablation threshold of 0.17 J/cm^2. This is a typical laser fluence. The ultrafast imaging under single pulse irradiation can better demonstrate the dynamic processes of HSFL formation.

Figure 5(a–d) shows two-dimensional Fourier transform (FT) images of the surface morphology at delay times of 100, 250, 700, and 850 ps, respectively. FT images are widely used to quantitatively describe periodic structures. The diffraction peak value Γ represents the period Λ (nm)=1000/ Γ (1/ μm), and the width corresponds to the variety range of the period, and the peak intensity reflects the uniformity and contrast of the periodic structures. During the formation and disappearance of HSFL, LSFL and HSFL are always coexisted. In order to quantitatively demonstrate the evolution of the HSFL and LSFL after laser radiation, we defined the ratio I of the peak intensity of high-frequency signals I_{HSFL} to low-frequency signals I_{LSFL}, as shown in Fig. 6. I_{HSFL} and I_{LSFL} are the maximum values of FT peaks come from Fig. 5. The results in Figs. 4–6 indicate that the evolution of the surface morphology under femtosecond laser irradiation underwent the following five stages:

A) 0–100 ps: LSFL begins to split and become uniform

As shown in Fig. 3, only the LSFL structures existed

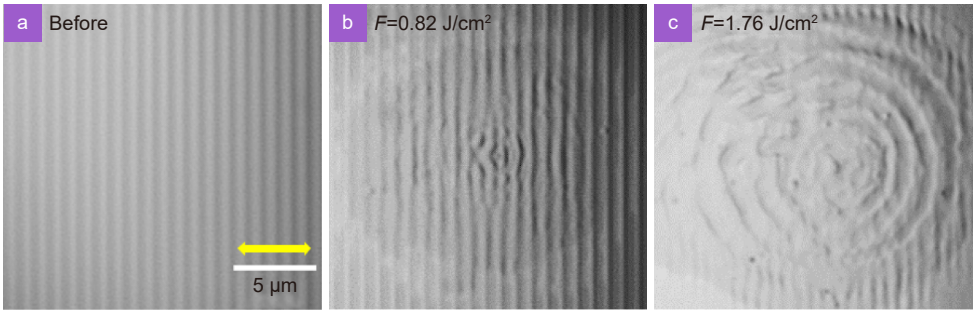

Fig. 3 | Optical images of surface microstructures before (**a**) and after (**b–c**) irradiation by a single laser pulse.

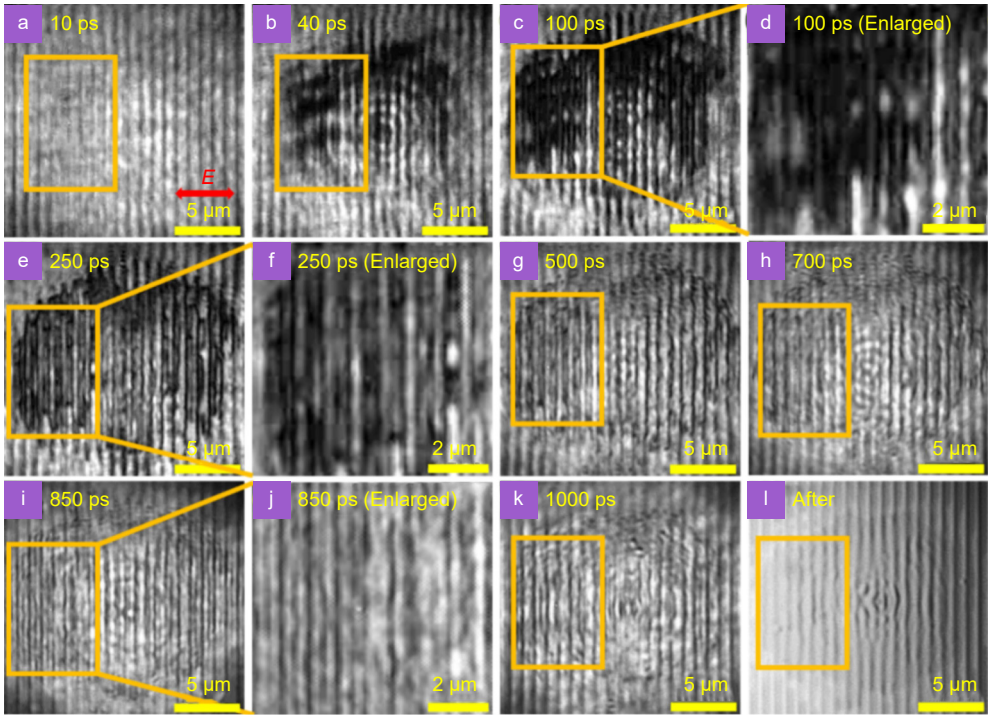

Fig. 4 | Optical micrographs of the silicon surface at different delay times after single-pulse laser irradiation. The horizontal double arrow shows the laser polarization direction.

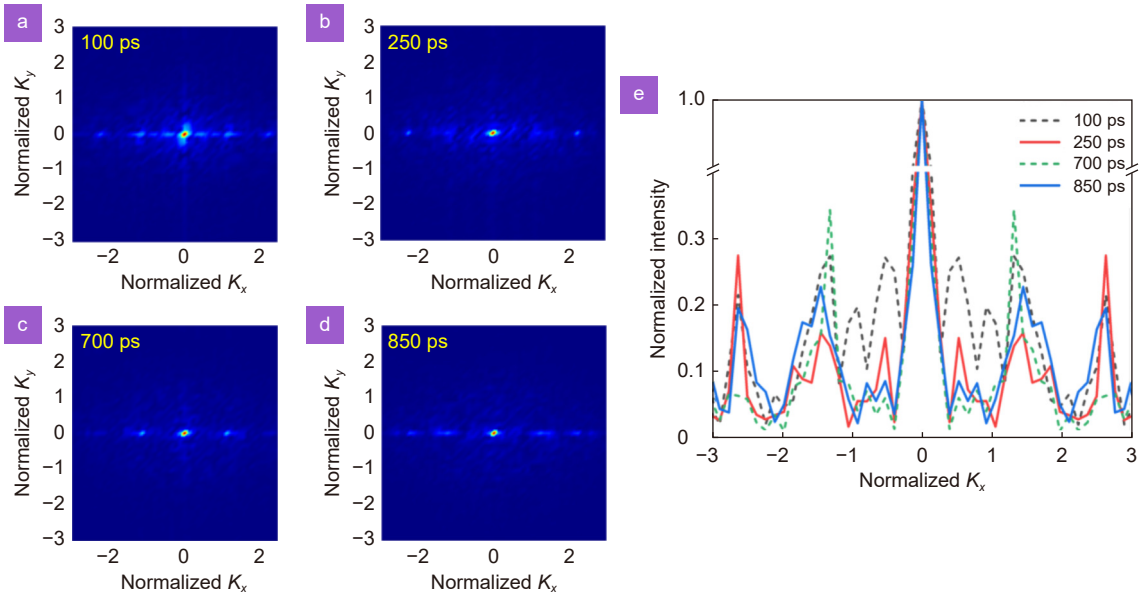

Fig. 5 | Two-dimensional FT images of the surface nanostructures shown in Fig. 4 at different delay times. (**a**) 100 ps, (**b**) 250 ps, (**c**) 700 ps, and (**d**) 850 ps, respectively. (**e**) The FT spectra in the *x*-direction of k_y=0.

before the pump beam reached the sample surface. Figure 4(a) shows that when the delay time is 10 ps, the ripples begin to split. Owing to the short evolution time of splitting, the ripples are relatively narrow and shallow and are blurred because of the absorption and scattering of the probe pulse by the ablation plume. The FT images show that the period of the split ripples is about 411.6 ± 53.1 nm, and the peak ratio of HSFL to LSFL signals is rapidly enhanced to 0.41.

Figure 4(b) shows that when the delay time is 40 ps, the image darkens, indicating that the surface is in a strong eruption state. The grooves at the split grew deeper and wider owing to the extrusion of the ejected plume and becomes evident and begin to be uniform in the transient optical image. The FT images show that the HSFL peak becomes more pronounced, and the ratio of

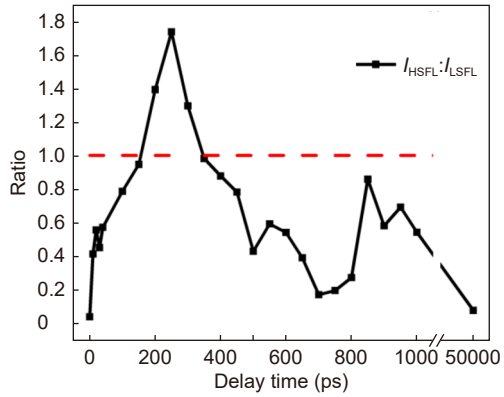

Fig. 6 | The delay time dependence of the peak intensity ratio of HSFL to LSFL corresponding to the FT images.

HSFL to LSFL increases to 0.57. Figure 4(c) and 4(d) show that when the delay time is 100 ps, the split ripples become more pronounced and uniform, and the original LSFL are less evident. The period of the HSFL is about 381 ± 46.9 nm, and the ratio of HSFL to LSFL increases to 0.79. The surface is still in a plasma eruption state and is very dark owing to the violent ablation plume[57].

B) 150–350 ps: Uniform HSFL

When the delay time is between 150–350 ps, the ejected plume diffuses into the nearby air and becomes thinner with less probe pulse absorption. The ripples gradually become clearer, indicating the end of the most intense ejection of the ablated materials. Figures 4–6 show that when the delay time is 250 ps, a uniform HSFL is formed with a period of 382 ± 39.8 nm. The HSFL dominates the surface morphology, whereas the LSFL almost disappears. The peak ratio of HSFL or LSFL reaches 1.73.

C) 400–700 ps: Uniform HSFL degenerates into an irregular LSFL

Figure 4(g) shows that when the delay time is 500 ps, the HSFLs are still relatively uniform, with a period of 380.5 ± 43.4 nm. However, due to thermal effects during ablation and melting, the ripples become slightly blurry and curved. The FT image shows that the HSFL peak begins to weaken, and the HSFL to LSFL ratio decreases to 0.59. Figure 4(h) shows that when the delay time is 700 ps, the further accumulation of thermal effects causes most of the HSFLs to disappear. However, unexpectedly, curved and shallow LSFL appear, and the image is very blurry. Figures 5 and 6 show that the HSFL signal peak is very weak, whereas the reappearing LSFL peak becomes very strong. The HSFL to LSFL ratio decreases to 0.19.

D) 750–850 ps: LSFL undergoes secondary splitting and evolves into weakly uniform HSFL

Figure 4(i) and 4(j) show that when the delay time is 850 ps, due to the continued weak ablation, splitting occurs again on the ridge of reappeared LSFL, forming weakly uniform HSFL. The HSFL to LSFL ratio increases to 0.85.

E) 900 ps solidification: The HSFL formed during the second splitting evolves into an LSFL

Figure 4(k) shows that when the delay time is 1000 ps, the re-split HSFL becomes curved and fractured over time and gradually transforms into an LSFL owing to thermal effects and fluid dynamics. The grooves of re-split HSFL are much narrower and shallower than those of LSFL, and they are more easily filled by the surface melt due to the thermos-hydrodynamic effect and surface tension. The FT image shows that the ratio of HSFL or LSFL has decreased to 0.54. Figure 4(l) shows that, after solidification, the split ripple disappeared, and only the curved and broken LSFL remains, with its width significantly narrowing. The ratio of HSFL or LSFL decreases to 0.08, approaching 0.

Overall, the HSFL originated from the splitting of the LSFL, which began at 5–10 ps. An intense ablation and ejection occurred before 150 ps. The enormous pressure during ablation caused the grooves of the split LSFL to widen, leading to a reduction in the pressure and narrowing of the original grooves, thereby promoting the uniformity of the split ripples. In the range of 150–350 ps, the ratio of the HSFL to LSFL signal peaks was greater than 1, indicating the formation of a uniform HSFL. Within a delay time of 400–700 ps, owing to the combined effects of the thermal effect and the viscous force of the original LSFL at the bottom, the HSFL becomes curved and fractured. The transient HSFL were continuously ablated and evolved into LSFL because the bottom LSFL was gradually observed. Within a delay time of 750–850 ps, the bottom LSFL underwent secondary splitting, forming a weakly uniform HSFL, where the LSFL and HSFL coexist. From a delay time of 900 ps to solidification, grooves formed during secondary splitting owing to melting and fluid effects.

Figure 4 clearly shows that transient HSFL structures mainly appear in the external region of the laser spot, while they are very unclear and unstable in the central region. Figure 2(c) and 2(d) show that there are several diffraction rings in the inner region, while in the outer region, the laser intensity changes smoothly without significant fluctuations. Therefore, the diffraction rings seriously disturb the formation of HSFL.

Ultrafast dynamics of the formation of HSFL induced by a single laser with different fluences

In the following section, we investigate the ultrafast processes of transient HSFL and LSFL induced by single-pulse laser irradiation with different fluences.

The formation of a transient HSFL induced by single-pulse laser irradiation with different fluences is shown in Fig. 7. To demonstrate the evolution of transient ripples briefly and clearly, only typical structures at the characteristic delay time are shown in the figures. When the laser fluence is 0.40 J/cm^2, only weak eruptions of ablated plumes are observed, and no splitting occurs on the LSFL.

When the laser fluence is 0.44 J/cm^2, due to the low laser fluence, splitting begins to occur very slowly. The LSFL at the center of the ablation area begins to split at a delay time of 100 ps. Within a delay time of 200–300 ps, as the ablation process continues, the split grooves become longer and clearer. Because of the influence of melting and fluid dynamics (surface tension), the split ripples become shorter and fewer during a delay time of 400–500 ps. When the delay time reaches 600 ps, almost all the split ripples disappear. When the delay time is 1500 ps, owing to the continuous weak ablation, the LSFL become thinner, and the grooves become wider, ultimately leaving only the LSFL.

When the laser fluence increased to 0.59 J/cm^2, clear and straight splitting of LSFL was observed in the range of 150–350 ps. The split ripples exhibited a trend of homogenization but did not form uniform HSFL. Within a delay time of 550–650 ps, owing to the influence of ablation and thermal effects, the split grooves gradually became shallower, and the ripples show obvious breaks and curves. When the delay time increased to 850 ps, the split ripples disappeared, and fuzzy and irregular LSFL appeared.

When the laser fluence further increased to 1.76 J/cm^2, strong ablation occurred in the range of 100–200 ps. The probe pulse was obscured by the ejected plume, resulting in very dark spots and blurred images, which are not presented here. At a delay time of 300 ps, the LSFL exhibited clear and straight splitting and began to

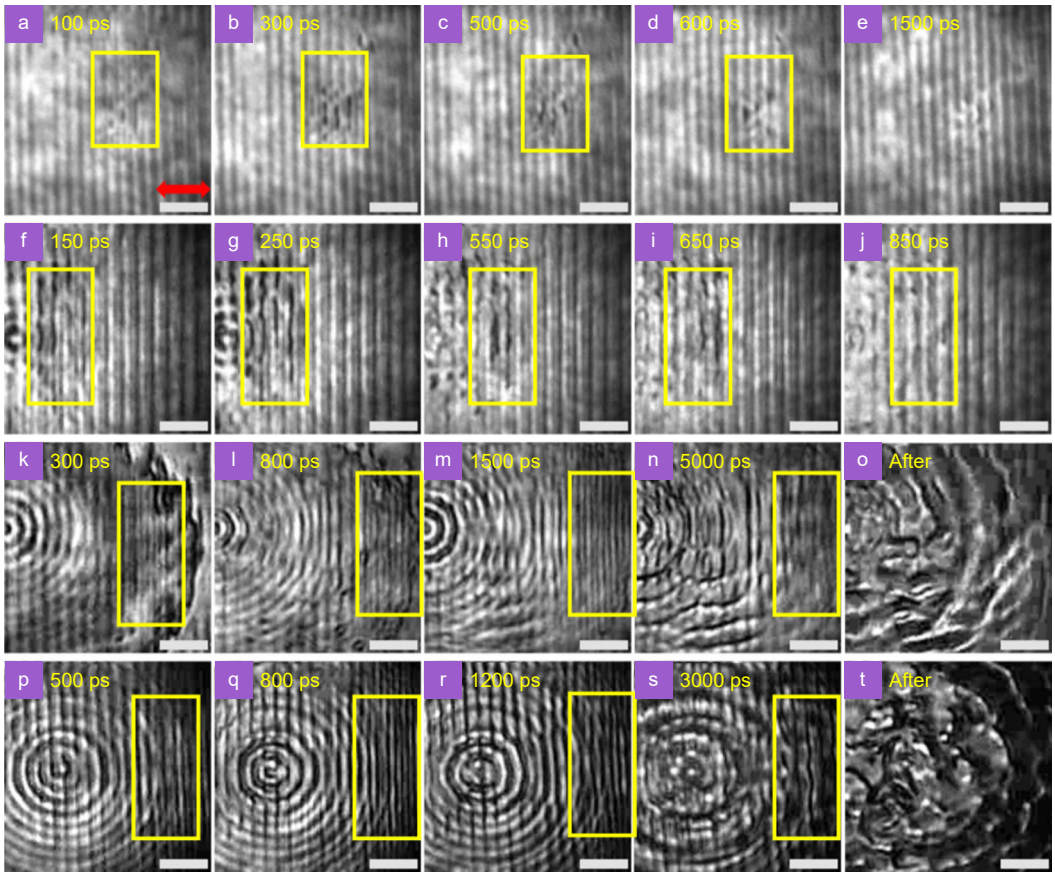

Fig. 7 | Optical micrographs of the silicon surface with pre-fabricated LSFL at different delay times after irradiation by a single laser pulse with different fluences. (**a–e**) Laser fluence is 0.44 J/cm^2, (**f–j**) is 0.59 J/cm^2, (**k–o**) is 1.76 J/cm^2, and (**p–t**) is 3.53 J/cm^2. The red horizontal double arrow shows the laser polarization direction. The gray scale in all figures is 3 microns.

homogenize. As the ablation continued, a regular and uniform HSFL was observed when the delay time was between 800–1500 ps. However, as the delay time increased further, the uniform HSFL gradually became blurred and shallower and began to curve and break. At a delay time of 5000 ps, the HSFL was severely ablated. Curved LSFL appear on the surface with obvious splitting. After solidification, all ripples, including the HSFL and LSFL, were completely submerged owing to intense thermal melting and hydrodynamic effects.

For a laser fluence of 3.53 J/cm^2, owing to the strong absorption and scattering of the probe light by the dense ejected plume, the transient images before a delay time of 300 ps were very dark, and the surface microstructures could not be observed. The split ripples begin to homogenize at a delay time of 500 ps and become a clear and uniform HSFL at a delay time of 800 ps. At a delay time of 1200 ps, the HSFL gradually became fuzzy and curved upon further ablation. At a delay time of 3000 ps, the ripples were completely ablated. Only twisted LSFL with split grooves were observed.

Figure 8 shows a clear and intuitive delay–time dependence of the five transient processes on the silicon surface irradiated by a single pulse with different laser fluences. No splitting of the LSFL occurred when the laser fluence was less than 0.4 J/cm^2. When the laser fluence increased to 0.44 J/cm^2, the splitting of LSFL occurred, but no homogenization happened. When the laser fluence was increased to 0.59 J/cm^2, HSFL homogenization occurred but was not completed; that is, no uniform HSFL appeared. When the laser fluence was in the range of 0.71–3.53 J/cm^2, the evolution process of the periodic structures was similar. Splitting of the LSFL emerged and eventually evolved into uniform HSFL. With continued ablation, the HSFL were ablated, and the surface morphology transitioned into curved and split LSFL, which eventually evolved into narrow, curved LSFL. When the laser fluence was greater than 1.76 J/cm^2, owing to intense thermal melting and fluid dynamics effects, the LSFL was submerged after solidification. Therefore, under an appropriate laser fluence of single-pulse irradiation, the splitting and homogenization of LSFL formed transient HSFL.

Figure 9 shows a statistical analysis of the periods of the transient HSFL under single-pulse irradiation with different laser fluences. The period of the HSFL, denoted by Λ_{HSFL}, was observed to be almost independent of the laser fluence and was determined to be $\Lambda_{\mathrm{HSFL}}=\Lambda_{\mathrm{LSFL}}/2$, where Λ_{LSFL} is the period of the prefabricated LSFL.

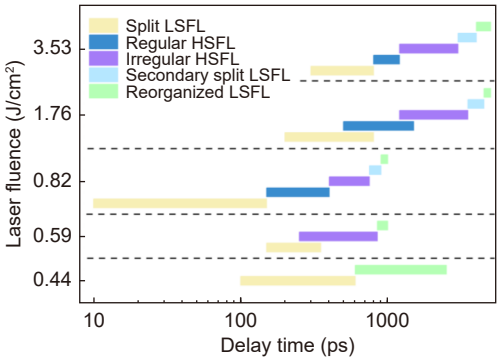

Fig. 8 | Evolution of surface morphology with delay time under single pulse irradiation with different laser fluences. LSFL was pre-fabricated prior to irradiation by a single pulse.

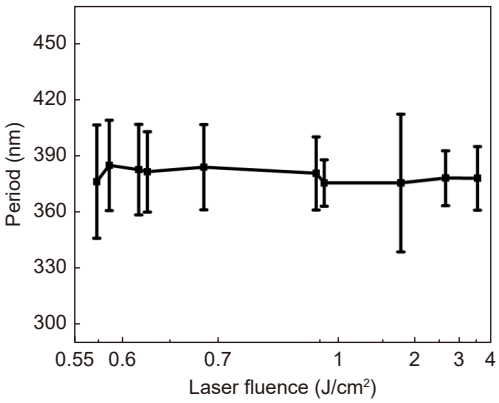

Fig. 9 | The laser fluence dependence of the period of uniform and clear HSFL under femtosecond laser irradiation.

Discussion: Ultrafast dynamics of the formation of HSFL

As its period is less than half the incident laser wavelength, HSFL is a processing method that breaks the diffraction limit. However, the interaction between the femtosecond laser and matter involves a series of complex physical processes, such as photon absorption, photoacoustic coupling and lattice heating, material ablation and Coulomb explosion, thermal shock waves, and fluid mechanics, rendering the HSFL formation mechanism unclear[58,59]. Although many studies have observed solidified HSFL using SEM, TEM, and AFM, and demonstrated the dependence of the HSFL period on the laser fluence, the origin and evolution process of HSFL is still not well understood. Based on the ultrafast imaging of transient HSFL on silicon surfaces with prefabricated LSFL, the mechanism of the origin and evolution of the HSFL are further discussed below.

Figures 4 and 6 show that after single-pulse laser irradiation with appropriate fluences, only the curved LSFL remained on the solidified surface. However, the ultrafast

imaging results indicate that these LSFL ridges undergo splitting and even homogenization of the HSFL. These split grooves are eventually buried owing to thermodynamic effects, leaving nano-voids and nano-gaps inside. During the manufacture of the LSFL using two-beam interference, the average accumulated pulse reached 25. Therefore, it can be inferred that the nano-cavities and nanogaps may remain in the LSFL ridge, as shown in Fig. 10(a–c).

During femtosecond laser excitation, significant local field enhancement occurs near these nano-cavities, which become local hotspots[60]. As shown in Fig. 4(b), narrow and deep slits were observed on the LSFL ridge at a delay time of 40 ps. As the delay time increased to 850 ps, as shown in Fig. 4(i), the LSFL still existed in a similar splitting state at the bottom after the top part of the ripples were ablated, indicating that nano-planes were formed within the material, as shown in Fig. 10(d). The strong local enhancement of the light field led to intense local ablation, and the enormous pressure generated by the ejected plume pushed the splitting ripples toward the grooves of the original LSFL, forming a uniform HSFL.

An air circle/ellipse is placed in the sub-surface layer at the LSFL ridges to represent the nano-cavities. To observe the transient response of the structural surface to the light field during femtosecond laser irradiation, we numerically simulated the transient process during femtosecond laser irradiation in steps of 0.1 fs. The simulation results indicate that strong localized enhancement of light field occur around the cavity. The nanocavity extends in the direction perpendicular to the sample surface and forms a deep and narrow nanoplane, which has a positive feedback effect with the local light field increasement[60]. The details of the numerical simulation are shown in the supplementary materials.

Yoann Levy et al. studied the relaxation dynamics of femtosecond-laser-induced temperature modulation on the surfaces of silicon with the two-dimensional two-temperature model[61]. The numerical results revealed that the lattice temperature modulation remained for longer than 50 ps, and suggested that the molten matter could be relocation toward LIPSS formation derived by the modulated temperature profile on the material surfaces.

Therefore, the local enhancement of the nanocavities in the LSFL ridge led to the splitting of the LSFL, and the thermodynamic effects drove the homogenization of the HSFL, as shown in Fig. 10(e–f).

The above discussion indicates that the local enhancement of the light field in the nano defects in the middle of the LSFL ridge plays a crucial role in the formation of transient HSFL. In order to study if there are nano defects in the LSFL ridge, the sample with prefabricated LSFL is put in HF solution with a concentration of 10%, and corroded for 90 minutes, and then cleaned with deionized water in an ultrasonic cleaner. The surface nanostructures were observed with SEM before and after etched with HF solution, as shown in Fig. 11. Regular LSFL gratings were observed in Fig. 11(a), and the enlarged image clearly shows that there are no nano defects in the LSFL ridge. However, after the sample was etched, different types of nano defects,such as nano holes, nano cracks appeared in the middle of the LSFL ridge, as shown in Fig. 11(c–f). The size of these nano defects mainly varies in the range of 10 to 60 nm. These results indicate that most of the transient grooves of HSFL were filled with melted material on the surface layer, leaving some nano cracks or nano cavities in the LSFL ridge.

If the laser fluence is increased to 0.24 J/cm^2, nanogrooves appeared directly in the middle of the LSFL ridges, as shown in Fig. 12. These nanogrooves are very narrow, only 10–70 nm wide, and obviously rather deep. This phenomenon is very similar to the nanoplanes inside fused silica, which originates from local enhancement of laser field near nanoplasma[35]. These experimental

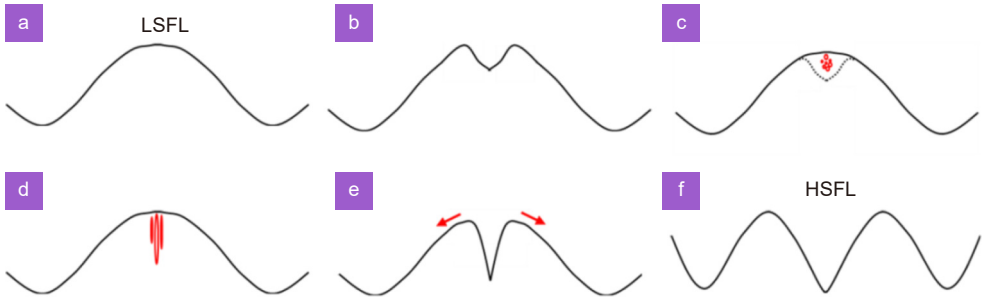

Fig. 10 | (**a–c**) Schematic diagram of the formation process of submerged nanocavities during LSFL prefabrication. (**d–f**) Schematic diagram of the formation of uniform HSFL.

results further demonstrate that after multiple pulses irradiation, there are nano cavities submerged in the middle of the ridge of LSFL.

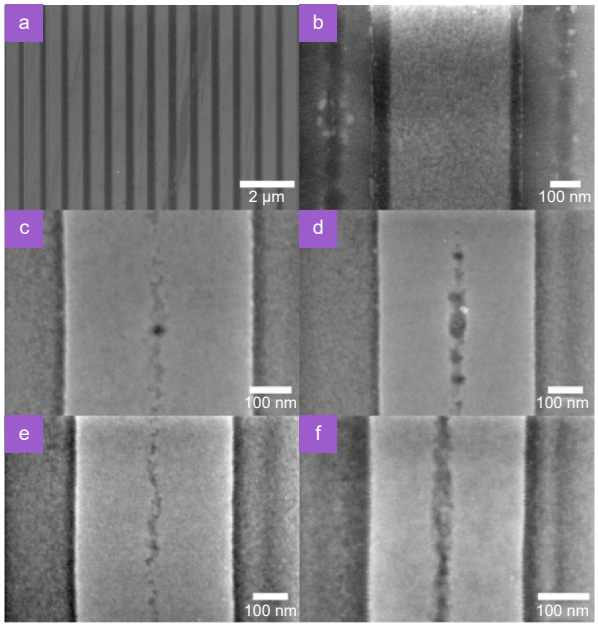

Fig. 11 | SEM images of the LSFL prefabricated on a silicon surface by direct writing with dual-beam interference, where a single-beam laser with a fluence of 0.13 J/cm² and a scanning speed of 2 mm/s. (**a**–**b**) Before etched, and (**c**–**f**) after etched with HF solution.

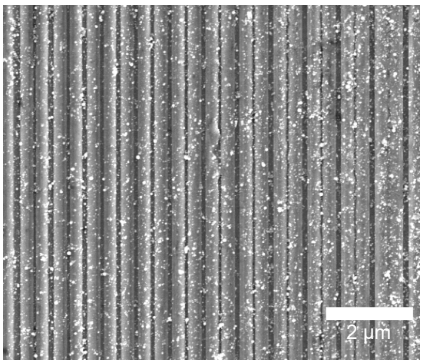

Fig. 12 | SEM image of silicon surface by direct writing with dual-beam interference, where a single-beam laser with a fluence of 0.24 J/cm² and a scanning speed of 2.0 mm/s. The sample was not corroded with HF solution.

The molten material backfilled into the HSFL groove solidified, resulted in a partially amorphous or polycrystalline state with a lot of defect sites. Compared to single-crystal silicon, the re-solidified material exhibited higher absorption rate. During laser irradiation, nanoscale plasmas in higher excited states are formed rapidly. Theoretical calculations indicate that the formation of nanoscale plasmas in the middle of LSFL ridges can further induces local field enhancement [see the Supplementary information]. The increased absorption rate of the information filled in the HSFL grooves, coupled with the positive feedback of local enhancement, leads to intense localized ablation, accords well the narrow and deep transient HSFL grooves observed in the experiments of ultrafast imaging.

The grooves of transient HSFL induced by a single pulse are very narrow. Due to the hydrodynamics of the molten layer driven by surface tension and diffusion, these transient grooves disappear after solidification. The central protrusion of the LSFL ripple will be reduced, and even shallow groove appears[52]. Meanwhile, a lot of defects, such as nanopores or nanogrooves, are submerged within the LSFL ridge, as shown in Fig. 12. Wang et al. reported that after corrosion with HF solution, Si surface exhibited very different internal structures, and even HSFL ripples[26]. These changes continuously accumulate under the multi pulse irradiation of femtosecond laser, leading to the evolution of LSFL into HSFL structures.

Experimental results of time-resolved shadowgraphs of material ejection after femtosecond laser pulse irradiation indicated that the ablated material typically undergo multiple intermittent eruptions[57,62,63], and the lasting time and interval of the eruptions are related to the pulse energy and material properties. The second eruption occurred usually with a delay time of 0.3–7.0 ns. The velocity of the ejected plume was very high, at a level of 10^5 m/s[57]. The corresponding inward expansion compressed the interior of the surface layer, and led to the conversion of thermal energy into mechanical energy, which caused thermoelastic waves and the material to spray at longer delay time. The second splitting of LSFL is mainly accompanied by a secondary eruption of ablative material. Similar to the first appearance of HSFL, it is also caused by local enhancement of laser field.

The phenomenon of secondary splitting is not very clear for the two reasons. One is that the second eruption is weaker, causing the grooves to become shallower during the secondary splitting. Secondly, the ripples are irregular due to the strong influence of thermal melting and fluid mechanics.

Conclusion

HSFL is usually induced by multiple femtosecond laser pulses, which makes the formation mechanism more complex because of several factors, such as deposited debris, a disturbed light field of the subsequent laser,

thermal accumulation, and hydrodynamic effects. In this study, we demonstrated for the first time the evolution of HSFL formation induced by a single femtosecond laser pulse using collinear pumped-probe imaging method. A regular LSFL with a period of 760 nm was fabricated in advance on a silicon surface with two-beam interference from an 800 nm femtosecond laser. The ultrafast dynamics of the HSFL formation on the silicon surface of a prefabricated LSFL under single-femtosecond laser pulse irradiation were studied. A common feature is that the evolution of the surface structure undergoes five sequential stages: the LSFL begins to split, becomes a uniform HSFL, degenerates into an irregular LSFL, undergoes secondary splitting into a weakly uniform HSFL, and evolves into an irregular LSFL or is submerged. By analyzing these results, it was proposed that the splitting of LSFL was caused by the local enhancement of the submerged nanocavities and the filled amorphous silicon in the transient nanogrooves in the middle of the prefabricated LSFL ridge, and the thermodynamic effect drove the homogenization of the splitting LSFL and evolved into HSFL.

References

1. Chichkov BN, Momma C, Nolte S, Von Alvensleben F, Tünnermann A. Femtosecond, picosecond and nanosecond laser ablation of solids. *Appl Phys A* **63**, 109–115 (1996).
2. Sugioka K, Cheng Y. Ultrafast lasers—reliable tools for advanced materials processing. *Light Sci Appl* **3**, e149 (2014).
3. Wang JC, Guo CL. Ultrafast dynamics of femtosecond laser-induced periodic surface pattern formation on metals. *Appl Phys Lett* **87**, 251914 (2005).
4. Zhang YC, Jiang QL, Cao KQ, Chen TQ, Cheng K et al. Extremely regular periodic surface structures in a large area efficiently induced on silicon by temporally shaped femtosecond laser. *Photonics Res* **9**, 05000839 (2021).
5. Jia TQ, Chen HX, Huang M, Zhao FL, Qiu JR et al. Formation of nanogratings on the surface of a ZnSe crystal irradiated by femtosecond laser pulses. *Phys Rev B* **72**, 125429 (2005).
6. Liu YY, Wang YX, Yang M, Wu Q, Li ZX et al. Deep-sub-wavelength ripples on the ZnO surface obtained via metal-film-assisted femtosecond laser processing. *Appl Surf Sci* **573**, 151576 (2022).
7. Zhang DS, Liu RJ, Li ZG. Irregular LIPSS produced on metals by single linearly polarized femtosecond laser. *Int J Extrem Manuf* **4**, 015102 (2022).
8. Li RH, Zhou YH, Liu ST, Huang M, Jiang SJ. Ink‐assisted laser‐induced heterogeneous permanent/erasable nanostructures on metals. *Laser Photonics Rev* **17**, 2200769 (2023).
9. Bricchi E, Klappauf BG, Kazansky PG. Form birefringence and negative index change created by femtosecond direct writing in transparent materials. *Opt Lett* **29**, 119–121 (2004).
10. Gu M, Li XP, Cao YY. Optical storage arrays: a perspective for future big data storage. *Light Sci Appl* **3**, e177 (2014).
11. Wu C, Crouch CH, Zhao L, Carey JE, Younkin R et al. Near-unity below-band-gap absorption by microstructured silicon. *Appl Phys Lett* **78**, 1850–1852 (2001).
12. Lopez‐Santos C, Puerto D, Siegel J, Macias‐Montero M, Florian C et al. Anisotropic resistivity surfaces produced in ITO films by laser‐induced nanoscale self‐organization. *Adv Opt Mater* **9**, 2001086 (2021).
13. Yong JL, Chen F, Yang Q, Jiang ZD, Hou X. A review of femtosecond-laser-induced underwater superoleophobic surfaces. *Adv Mater Interfaces* **5**, 1701370 (2018).
14. Jiang QL, Chen L, Liu JK, Zhang YC, Zhang SA et al. Periodic transparent nanowires in ITO film fabricated via femtosecond laser direct writing. *Opto-Electron Sci* **2**, 220002 (2023).
15. Chen L, Cao KQ, Li YL, Liu JK, Zhang SA et al. Large-area straight, regular periodic surface structures produced on fused silica by the interference of two femtosecond laser beams through cylindrical lens. *Opto-Electron Adv* **4**, 200036 (2021).
16. Li YH, Zhang XY, Zou TT, Mu QQ, Yang JJ. Vivid structural color macropatterns created by flexible nanopainting of ultrafast lasers. *ACS Appl Mater Interfaces* **14**, 21758–21767 (2022).
17. Buividas R, Mikutis M, Juodkazis S. Surface and bulk structuring of materials by ripples with long and short laser pulses: Recent advances. *Prog Quantum Electron* **38**, 119–156 (2014).
18. Bonse J, Hohm S, Kirner SV, Rosenfeld A, Kruger J. Laser-Induced Periodic Surface Structures-A Scientific Evergreen. *IEEE J Sel Top Quantum Electron* **23**, 15 (2017).
19. Huang M, Zhao FL, Cheng Y, Xu NS, Xu ZZ. Origin of laser-induced near-subwavelength ripples: interference between surface plasmons and incident laser. *ACS Nano* **3**, 4062–4070 (2009).
20. Sipe JE, Young JF, Preston JS, van Driel HM. Laser-induced periodic surface structure. I. Theory. *Phys Rev B* **27**, 1141–1154 (1983).
21. Bonse J, Munz M, Sturm H. Structure formation on the surface of indium phosphide irradiated by femtosecond laser pulses. *J Appl Phys* **97**, 013538 (2005).
22. Bonse J, Gräf S. Ten open questions about laser-induced periodic surface structures. *Nanomaterials* **11**, 3326 (2021).
23. Cheng K, Liu JK, Cao KQ, Chen L, Zhang YC et al. Ultrafast dynamics of single-pulse femtosecond laser-induced periodic ripples on the surface of a gold film. *Phys Rev B* **98**, 184106 (2018).
24. Okamuro K, Hashida M, Miyasaka Y, Ikuta Y, Tokita S et al. Laser fluence dependence of periodic grating Hashida structures formed on metal surfaces under femtosecond laser pulse irradiation. *Phys Rev B* **82**, 165417 (2010).
25. Miyaji G, Miyazaki K. Origin of periodicity in nanostructuring on thin film surfaces ablated with femtosecond laser pulses. *Opt Express* **16**, 16265–16271 (2008).
26. Wang L, Xu BB, Cao XW, Li QK, Tian WJ et al. Competition between subwavelength and deep-subwavelength structures ablated by ultrashort laser pulses. *Optica* **4**, 637–642 (2017).
27. Xie HB, Zhao B, Cheng JL, Chamoli SK, Zou TT et al. Super-regular femtosecond laser nanolithography based on dual-interface plasmons coupling. *Nanophotonics* **10**, 3831–3842 (2021).
28. Derrien TJY, Koter R, Krüger J, Höhm S, Rosenfeld A et al. Plasmonic formation mechanism of periodic 100-nm-structures upon femtosecond laser irradiation of silicon in water. *J Appl Phys* **116**, 074902 (2014).
29. Reif J, Costache F, Henyk M, Pandelov SV. Ripples revisited:

non-classical morphology at the bottom of femtosecond laser ablation craters in transparent dielectrics. *Appl Surf Sci* **197–198**, 891–895 (2002).
30. Costache F, Henyk M, Reif J. Modification of dielectric surfaces with ultra-short laser pulses. *Appl Surf Sci* **186**, 352–357 (2002).
31. Reif J, Varlamova O, Costache F. Femtosecond laser induced nanostructure formation: self-organization control parameters. *Appl Phys A* **92**, 1019–1024 (2008).
32. Ionin AA, Kudryashov SI, Ligachev AE, Makarov SV, Seleznev LV et al. Nanoscale cavitation instability of the surface melt along the grooves of one-dimensional nanorelief gratings on an aluminum surface. *JETP Lett* **94**, 266–269 (2011).
33. Nathala CSR, Ajami A, Ionin AA, Kudryashov SI, Makarov SV et al. Experimental study of fs-laser induced sub-100-nm periodic surface structures on titanium. *Opt Express* **23**, 5915–5929 (2015).
34. Abere MJ, Torralva B, Yalisove SM. Periodic surface structure bifurcation induced by ultrafast laser generated point defect diffusion in GaAs. *Appl Phys Lett* **108**, 153110 (2016).
35. Bhardwaj VR, Simova E, Rajeev PP, Hnatovsky C, Taylor RS et al. Optically produced arrays of planar nanostructures inside fused silica. *Phys Rev Lett* **96**, 057404 (2006).
36. Pan AF, Wang WJ, Liu B, Mei XS, Yang HZ et al. Formation of high-spatial-frequency periodic surface structures on indium-tin-oxide films using picosecond laser pulses. *Mater Des* **121**, 126–135 (2017).
37. Zhang H, Du K, Li XW. Enhancement and blueshift of high-frequency laser-induced periodic surface structures with preformed nanoscale surface roughness. *Opt Express* **27**, 19973–19983 (2019).
38. Li C, Cheng GH, Sedao X, Zhang W, Zhang H et al. Scattering effects and high-spatial-frequency nanostructures on ultrafast laser irradiated surfaces of zirconium metallic alloys with nanoscaled topographies. *Opt Express* **24**, 1558–1568 (2016).
39. Zhang H, Colombier JP, Li C, Faure N, Cheng GH et al. Coherence in ultrafast laser-induced periodic surface structures. *Phys Rev B* **92**, 174109 (2015).
40. Huang M, Cheng Y, Zhao FL, Xu ZZ. The significant role of plasmonic effects in femtosecond laser-induced grating fabrication on the nanoscale. *Ann Phys-Berlin* **525**, 74–86 (2013).
41. Huang M, Xu ZZ. Spontaneous scaling down of femtosecond laser-induced apertures towards the 10-nanometer level: the excitation of quasistatic surface plasmons. *Laser Photonics Rev* **8**, 633–652 (2014).
42. Dufft D, Rosenfeld A, Das SK, Grunwald R, Bonse J. Femtosecond laser-induced periodic surface structures revisited: a comparative study on ZnO. *J Appl Phys* **105**, 034908 (2009).
43. Rudenko A, Abou-Saleh A, Pigeon F, Mauclair C, Garrelie F et al. High-frequency periodic patterns driven by non-radiative fields coupled with Marangoni convection instabilities on laser-excited metal surfaces. *Acta Mater* **194**, 93–105 (2020).
44. Rudenko A, Mauclair C, Garrelie F, Stoian R, Colombier JP. Amplification and regulation of periodic nanostructures in multipulse ultrashort laser-induced surface evolution by electromagnetic-hydrodynamic simulations. *Phys Rev B* **99**, 235412 (2019).
45. Skolski JZP, Römer GRBE, Vincenc Obona J, Huis in 't Veld AJ. Modeling laser-induced periodic surface structures: finite-difference time-domain feedback simulations. *J Appl Phys* **115**, 103102 (2014).
46. Zhou K, Jia X, Jia TQ, Cheng K, Cao KQ et al. The influences of surface plasmons and thermal effects on femtosecond laser-induced subwavelength periodic ripples on Au film by pump-probe imaging. *J Appl Phys* **121**, 104301 (2017).
47. Xu J, Min CJ, Zhang YQ, Ni JL, Cao GW et al. Imaging ultrafast evolution of subwavelength-sized topography using single-probe structured light microscopy. *Photonics Res* **10**, 1900–1908 (2022).
48. Obara G, Shimizu H, Enami T, Mazur E, Terakawa M et al. Growth of high spatial frequency periodic ripple structures on SiC crystal surfaces irradiated with successive femtosecond laser pulses. *Opt Express* **21**, 26323–26334 (2013).
49. Cao KQ, Chen L, Wu HC, Liu JK, Cheng K et al. Large-area commercial-grating-quality subwavelength periodic ripples on silicon efficiently fabricated by gentle ablation with femtosecond laser interference via two cylindrical lenses. *Opt Laser Technol* **131**, 106441 (2020).
50. Jia X, Jia TQ, Peng NN, Feng DH, Zhang SA et al. Dynamics of femtosecond laser-induced periodic surface structures on silicon by high spatial and temporal resolution imaging. *J Appl Phys* **115**, 143102 (2014).
51. Liu JK, Jia X, Wu WS, Cheng K, Feng DH et al. Ultrafast imaging on the formation of periodic ripples on a Si surface with a prefabricated nanogroove induced by a single femtosecond laser pulse. *Opt Express* **26**, 6302–6315 (2018).
52. Hou SS, Huo YY, Xiong PX, Zhang Y, Zhang SA et al. Formation of long- and short-periodic nanoripples on stainless steel irradiated by femtosecond laser pulses. *J Phys D Appl Phys* **44**, 505401 (2011).
53. Zhang YH, Jiang QL, Long MQ, Han RZ, Cao KQ et al. Femtosecond laser-induced periodic structures: mechanisms, techniques, and applications. *Opto-Electron Sci* **1**, 220005 (2022).
54. Yu XH, Qi DF, Wang HY, Zhang YW, Wang LT et al. In situ and ex-situ physical scenario of the femtosecond laser-induced periodic surface structures. *Opt Express* **27**, 10087–10097 (2019).
55. Lin XM, Li XH, Zhang YB, Xie CX, Liu KJ et al. Periodic structures on germanium induced by high repetition rate femtosecond laser. *Opt Laser Technol* **101**, 291–297 (2018).
56. Li ZX, Wu Q, Jiang XD, Zhou X, Liu YY et al. Formation mechanism of high spatial frequency laser-induced periodic surface structures and experimental support. *Appl Surf Sci* **580**, 152107 (2022).
57. Zhang N, Zhu XN, Yang JJ, Wang XL, Wang MW. Time-resolved shadowgraphs of material ejection in intense femtosecond laser ablation of aluminum. *Phys Rev Lett* **99**, 167602 (2007).
58. Nolte S, Momma C, Jacobs H, Tünnermann A, Chichkov BN et al. Ablation of metals by ultrashort laser pulses. *J Opt Soc Am B* **14**, 2716–2722 (1997).
59. Ionin AA, Kudryashov SI, Samokhin AA. Material surface ablation produced by ultrashort laser pulses. *Phys Usp* **60**, 149–160 (2017).
60. Huang M, Zhao FL, Cheng Y, Xu NS, Xu ZZ. Mechanisms of ultrafast laser-induced deep-subwavelength gratings on graphite and diamond. *Phys Rev B* **79**, 125436 (2009).
61. Levy Y, Derrien TJY, Bulgakova NM, Gurevich EL, Mocek T. Relaxation dynamics of femtosecond-laser-induced temperature modulation on the surfaces of metals and semiconductors. *Appl Surf Sci* **374**, 157–164 (2016).
62. Zhang TY, Guo BS, Jiang L, Chen ML, Zhan NW. Ultrafast observation of multiple shock waves evolution and interaction pro-

cesses in femtosecond laser processing. *Phys Fluids* **35**, 057114 (2023).

63. Liu JK, Zhao H, Cheng K, Ju JQ, Feng DH et al. Ultrafast dynamics of the thin surface plasma layer and the periodic ripples formation on GaP crystal irradiated by a single femtosecond laser pulse. *Opt Express* **27**, 37859–37876 (2019).

Acknowledgements

We are grateful for financial supports from the National Natural Science Foundation of China (12074123, 12174108), and the Foundation of 'Manufacturing beyond limits' of Shanghai, and 'Talent Program' of Henan Academy of Sciences.

Author contributions

All authors commented on the manuscript.

RZ Han performed the experiment and measurements under the guidance of TQ Jia. YC Zhang, QL Jiang helped to complete some of the experiments and discuss. L Chen and KQ Cao provided supplementary assistance in conducting additional experiments. SA Zhang, DH Feng, ZR Sun gave important suggestions to this work

Competing interests

The authors declare no competing financial interests.

Supplementary information

Supplementary information for this paper is available at https://doi.org/10.29026/oes.2024.230013